

Review of Band Structures for Fourteen Semiconductors of the Diamond and Zinc-blende Structures

Author: Eric Vidal **Supervisor:** Alain Dereux

1 Introduction

In this work, the main objective is to compute the electron band structure of face-centered cubic (FCC) semiconductors, also known as diamond crystal structure, and for zinc-blende structure. For this purpose, the pseudopotential form factors used are the ones from the seminal study presented by Cohen and Bergstresser¹. Therefore, the reference graphics to compare are also extracted from this research mentioned.

The model for computing the band structures is based on the Bloch model. Its main success is to compute the spectrum of the electron energy states by adding one new feature with respect to the Sommerfeld model in the one-electron approximation, the use of a periodic potential independent of time,

$$V(\mathbf{r}) = V(\mathbf{r} + \mathbf{R}_n) \quad (1)$$

where \mathbf{r} is the vector position, and \mathbf{R}_n is a vector in the direct lattice. This allows the expansion in a Fourier Series for the *pseudopotential* to perform the study in the reciprocal space,

$$V(\mathbf{r}) = \sum_{\mathbf{G}} V_{\mathbf{G}} e^{i \mathbf{G} \cdot \mathbf{r}} \quad (2)$$

where \mathbf{G} is a vector in the reciprocal lattice, and $V_{\mathbf{G}}$ in this case is the form factor for the FCC structure,

$$V_{\mathbf{G}} = V_{|\mathbf{G}|^2}^S \cos \mathbf{G} \cdot \mathbf{s} + i V_{|\mathbf{G}|^2}^A \sin \mathbf{G} \cdot \mathbf{s} \quad (3)$$

where $s = \frac{a}{8}(1, 1, 1)$ and \mathbf{s} are the positions for the 2 atoms relative to the primitive cell's center, and $V_{|\mathbf{G}|^2}^S$ and $V_{|\mathbf{G}|^2}^A$ are experimental fits from Table II in Cohen¹ et al.

This hypothesis allows us to find the Schrödinger equation in the reciprocal space to find the eigenvalues and eigenfunctions. This leads to the equations system of $\mathcal{N} \times \mathcal{N}$, where \mathcal{N} is the number of vectors for both the direct and reciprocal space, expressed using matrices as,

$$[\bar{H}(\mathbf{k}) - IE] \bar{c}(\mathbf{k}) = 0 \quad (4)$$

which contains the hermitian matrix to diagonalize resulting in the eigenvalues, $E_{\lambda}(\mathbf{k})$, and eigenfunctions, $\psi_{\lambda, \mathbf{k}}(\mathbf{r})$ we were looking for. Finally, the Bloch functions, $u_{\lambda, \mathbf{k}}(\mathbf{r}) = u_{\lambda, \mathbf{k}}(\mathbf{r} + \mathbf{R}_n)$ could be derived as they mimic the reciprocal lattice periodicity in the direct lattice, plus define the Bloch wavefunctions, $\psi_{\lambda, \mathbf{k}}(\mathbf{r}) = u_{\lambda, \mathbf{k}}(\mathbf{r})e^{i \mathbf{k} \cdot \mathbf{r}}$ with $\mathbf{k} \in BZ$.

2 Methods

The general procedure for computing the BZ path in the standard direction for FCC structures is explained by Monkhorst and Pack². Following the path they paved, we perform a cutoff so if the vectors in the reciprocal lattice $|\mathbf{G}|^2 > 11(4\pi^2/a^2)$ units), $V_{\mathbf{G}} = 0$. Apart from that, $\forall |\mathbf{G}|^2 \leq 21$, thus with these conditions we already can

compute the BZ path, assign the spacing, a , for each semiconductor, and generate the vectors of the reciprocal lattice. Then, the following step is acquiring the pseudopotential parameters, compute the truncated representation of the Hamiltonian in the reciprocal space, and diagonalizing it to obtain the eigenvalues and eigenvectors. In fact, what is obtained are the band structures ready to be saved and plotted.

3 Results and Discussion

For the sake of the comparison, the point Γ of the semiconductors is studied to set its maximum as the 0 of energy by adjusting the coefficients $V_{\mathbf{G}=0}$. Such that the simulations generated and the plots from Cohen et al. can be compared, as well as setting the energy units in eV.

As we can appreciate the materials they studied and have been simulated in this work are Fig. 1 Si, Fig. 2 Ge, Fig. 3 Sn, Fig. 4 GaP, Fig. 5 GaAs, Fig. 6 AlSb, Fig. 7 InP, Fig. 8 GaSb, Fig. 9 InAs, Fig. 10 InSb, Fig. 11 ZnS, Fig. 12 ZnSe, Fig. 13 ZnTe, and Fig. 14 CdTe.

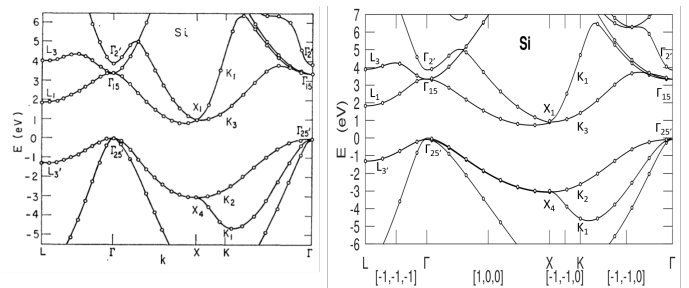


Fig. 1 Right: The band structure of Si extracted from Cohen et al. work along the standard direction of exploration for its BZ. **Left:** The simulated band structure of Si based on the pseudopotential from Cohen et al. work along the standard direction of exploration for its BZ.

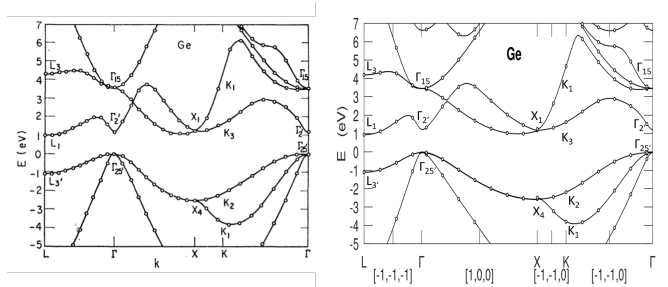


Fig. 2 Right: The band structure of Ge extracted from Cohen et al. work along the standard direction of exploration for its BZ. **Left:** The simulated band structure of Ge based on the pseudopotential from Cohen et al. work along the standard direction of exploration for its BZ.

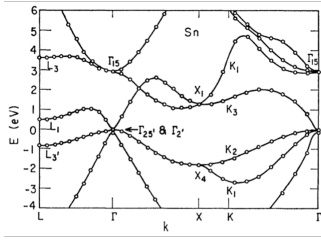


Fig. 3 Right: The band structure of Sn extracted from Cohen et al. works along the standard direction of exploration for its BZ. **Left:** The simulated band structure of Sn based on the pseudopotential from Cohen et al. work along the standard direction of exploration for its BZ.

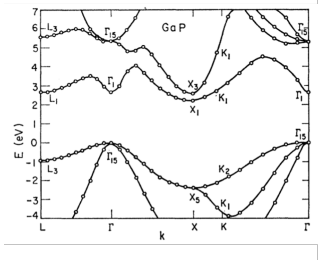
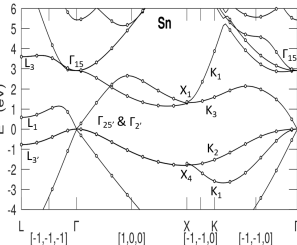


Fig. 4 Right: The band structure of GaP extracted from Cohen et al. work along the standard direction of exploration for its BZ. **Left:** The simulated band structure of GaP based on the pseudopotential from Cohen et al. work along the standard direction of exploration for its BZ.

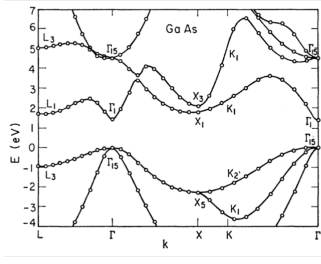
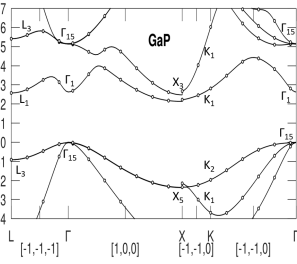


Fig. 5 Right: The band structure of GaAs extracted from Cohen et al. work along the standard direction of exploration for its BZ. **Left:** The simulated band structure of GaAs based on the pseudopotential from Cohen et al. work along the standard direction of exploration for its BZ.

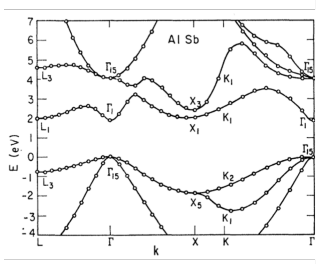
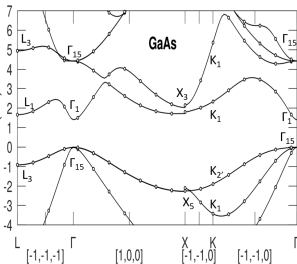


Fig. 6 Right: The band structure of AlSb extracted from Cohen et al. work along the standard direction of exploration for its BZ. **Left:** The simulated band structure of AlSb based on the pseudopotential from Cohen et al. work along the standard direction of exploration for its BZ.

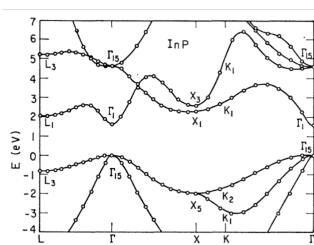
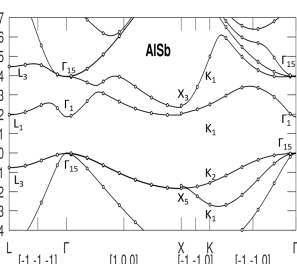


Fig. 7 Right: The band structure of InP extracted from Cohen et al. works along the standard direction of exploration for its BZ. **Left:** The simulated band structure of InP based on the pseudopotential from Cohen et al. work along the standard direction of exploration for its BZ.

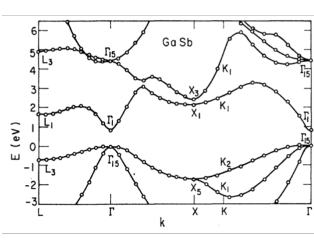
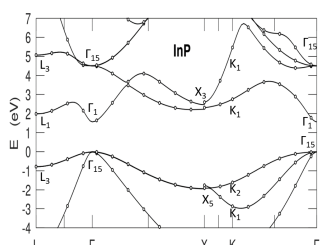


Fig. 8 Right: The band structure of GaSb extracted from Cohen et al. work along the standard direction of exploration for its BZ. **Left:** The simulated band structure of GaSb based on the pseudopotential from Cohen et al. work along the standard direction of exploration for its BZ.

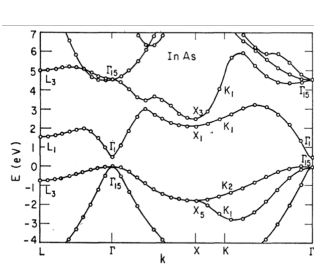
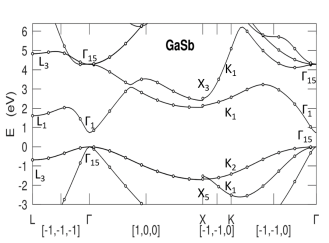


Fig. 9 Right: The band structure of InAs extracted from Cohen et al. work along the standard direction of exploration for its BZ. **Left:** The simulated band structure of InAs based on the pseudopotential from Cohen et al. work along the standard direction of exploration for its BZ.

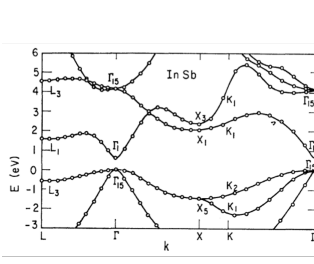
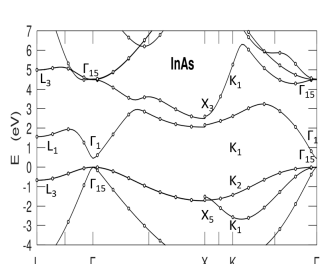
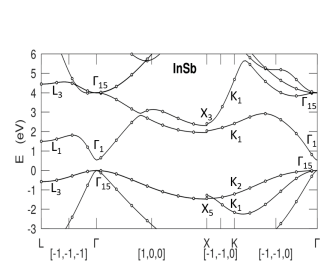


Fig. 10 Right: The band structure of InSb extracted from Cohen et al. work along the standard direction of exploration for its BZ. **Left:** The simulated band structure of InSb based on the pseudopotential from Cohen et al. work along the standard direction of exploration for its BZ.



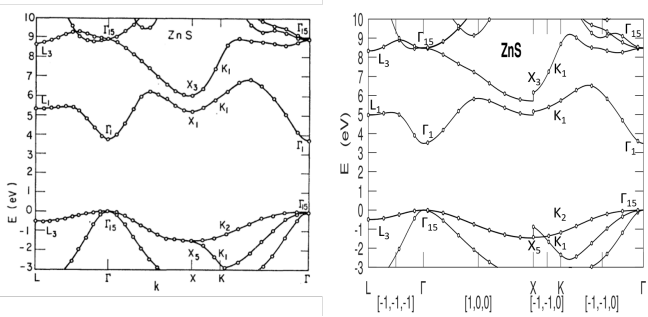


Fig. 11 Right: The band structure of ZnS extracted from Cohen et al. work along the standard direction of exploration for its BZ. **Left:** The simulated band structure of ZnS based on the pseudopotential from Cohen et al. work along the standard direction of exploration for its BZ.

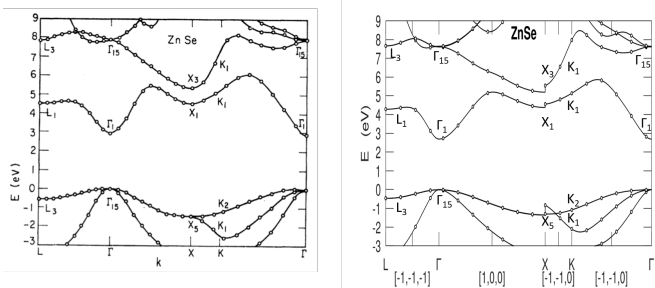


Fig. 12 Right: The band structure of ZnSe extracted from Cohen et al. work along the standard direction of exploration for its BZ. **Left:** The simulated band structure of ZnSe based on the pseudopotential from Cohen et al. work along the standard direction of exploration for its BZ.

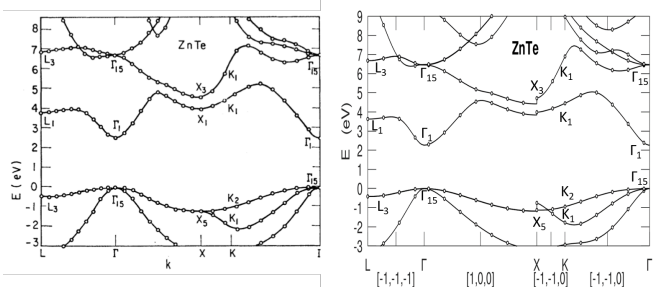


Fig. 13 Right: The band structure of ZnTe extracted from Cohen et al. work along the standard direction of exploration for its BZ. **Left:** The simulated band structure of ZnTe based on the pseudopotential from Cohen et al. work along the standard direction of exploration for its BZ.

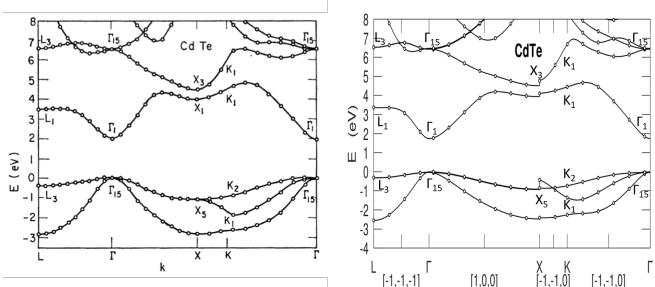


Fig. 14 Right: The band structure of CdTe extracted from Cohen et al. work along the standard direction of exploration for its BZ. **Left:** The simulated band structure of CdTe based on the pseudopotential from Cohen et al. work along the standard direction of exploration for its BZ.

4 Conclusion

In terms of the comparison between the reference paper and the simulations produced, we can determine that is a complete success. All the graphics show behaviors completely equal in both situations, although for heavy components the simulation can have a slight discontinuity in the point X for the simulation.

However, it is true that in some cases it can be observed how some new bands show up for the simulated case. It is likely that in the reference paper, they did not study further than what they plotted, in contrast to what is simulated that goes far beyond up to 16 band structures. What matters is that the main features are accomplished, such as the split of X_1 into X_1 and X_3 for homopolar substances, the Γ_2' level decreasing its energy for heavier semiconductors, as well as L_1 going down with respect to the X_1 level.

Overall, it is a great success that reaffirms the validity of the Bloch model for a broad range of semiconductors showing an FCC structure.

References

- 1 Cohen, M. L. and Bergstresser, T. K. (1966). Band structures and pseudopotential form factors for fourteen semiconductors of the diamond and zinc-blende structures. *Phys. Rev.*, 141:789–796.
- 2 Monkhorst, H. J. and Pack, J. D. (1976). Special points for brillouin-zone integrations. *Phys. Rev. B*, 13:5188–5192.